Editors' Suggestion

Spin-Momentum-Locked Edge Mode for Topological Vortex Lasing

Zhen-Qian Yang,[1,2] Zeng-Kai Shao,[1,2] Hua-Zhou Chen,[1,2] Xin-Rui Mao,[1,2] and Ren-Min Ma[1,2,*]
[1]*State Key Lab for Mesoscopic Physics and School of Physics, Peking University, Beijing, China*
[2]*Frontiers Science Center for Nano-optoelectronics & Collaborative Innovation Center of Quantum Matter, Beijing, China*

(Received 4 March 2020; accepted 3 June 2020; published 1 July 2020)

Spin-momentum locking is a direct consequence of bulk topological order and provides a basic concept to control a carrier's spin and charge flow for new exotic phenomena in condensed matter physics. However, up to date the research on spin-momentum locking solely focuses on its in-plane transport properties. Here, we report an emerging out-of-plane radiation feature of spin-momentum locking in a non-Hermitian topological photonic system and demonstrate a high performance topological vortex laser based on it. We find that the gain saturation effect lifts the degeneracy of the paired counterpropagating spin-momentum-locked edge modes enabling lasing from a single topological edge mode. The near-field spin and orbital angular momentum of the topological edge mode lasing has a one-to-one far-field radiation correspondence. The methodology of probing the near-field topology feature by far-field lasing emission can be used to study other exotic phenomena. The device can lead to applications in superresolution imaging, optical tweezers, free-space optical sensing, and communication.

DOI: 10.1103/PhysRevLett.125.013903

Introduction.—The surface of topological insulators hosts a new class of carriers of helical Dirac fermions with spin-momentum locking, where the carrier spin is locked at right angles to the carrier momentum [1,2]. Spin-momentum locking prevents backscattering between states of opposite momenta with opposite spins [3–5]. These exotic carriers are also great candidates for potential quantum computing and spintronic applications when superconductivity and magnetism are introduced to them via the proximity effect [6–12]. In 2008, Haldane and Raghu introduced band topology to the realm of photonics [13,14]. In the past decade, topological photonics has drawn substantial research attention, where spin-momentum locking also plays an essential role and has overturned some of the conventional views on light generation, propagation, and manipulation in both quantum and classical electromagnetic regimes [15–19]. In the quantum regime, a quantum emitter can efficiently couple to topological edge states and correlate its spin to the propagation direction via spin-momentum locking [20], which could lead to exotic photonic phenomena such as large-scale superradiant states [21,22], chiral spin networks [23,24], and topologically protected biphoton states [25]. In classical regimes, spin-momentum locking has been used to construct robust photonic waveguides immune to bending and defects [26–29], high quality optical cavities with arbitrary geometries [30–32], and novel laser devices with large area coherence and flexible reconfiguration [33–35]. However, to date the research on spin-momentum locking solely focuses on its in-plane transport properties. Yet the out-of-plane radiation property of spin-momentum locking has remained unexplored. In contrast to electronic system, a photonic system is naturally non-Hermitian because of the existence of gain and/or loss. The non-Hermitian gives another degree of freedom for manipulating light and endorses topological photonics' unique properties to its electronic counterpart [36–41].

Here, we use a topological photonic crystal to construct a band structure distinct in topology and demonstrate a high performance topological vortex laser boosted by spin-momentum locking. We reveal that spin-momentum locking not only protects in-plane unidirectional wave propagation for effective resonance, but also decouples the radiation direction from the resonant plane for directionally surface emitting. The immune of backscattering is verified by the identical lasing emission wavelength of the two topological edge modes with opposite spin. We find that the gain saturation effect enables individual lasing from a single topological edge mode resulting in a flow of pure photonic spin. The near-field spin and orbital angular momentum of the topological edge mode can be probed via the circularly polarized vortex beam of far-field lasing radiation. The high-performance lasing is featured with single mode operation with a high side-mode suppression ratio, compact footprint, low threshold, narrow emission linewidth, and vertical emission directionality [42].

Operation principle.—Figures 1(a) and 1(b) show the SEM images of a topological vortex laser with a ⋇-shaped topological interface which is fabricated by a standard nanofabrication process on a InGaAsP multiple quantum wells (MQWs) membrane [42]. We choose the complicated cavity geometry with bends for demonstrating the immune of backscattering of the topological edge states. The immune of backscattering is protected by spin-momentum locking,

 © 2020 American Physical Society

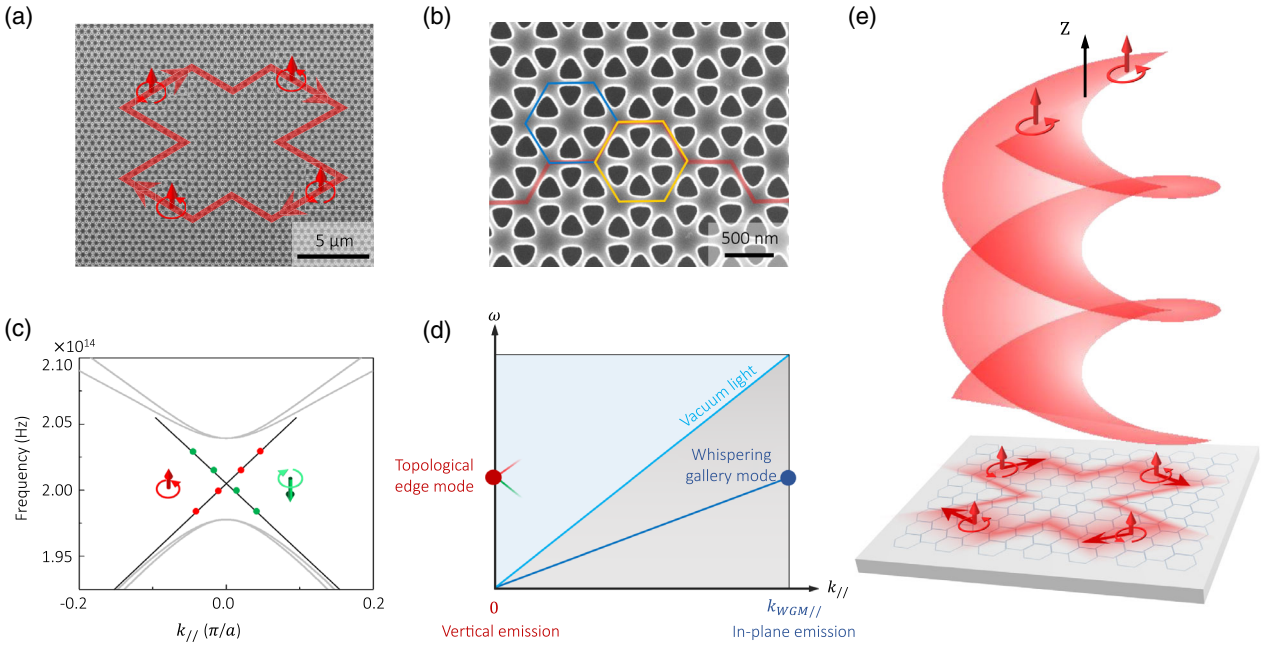

FIG. 1. Operation principle of the topological vortex laser. (a) SEM image of a topological vortex laser with a ⋈-shaped cavity indicated by the red line and arrows. The corresponding spin direction of the cavity mode is indicated by the out-of-plane arrows. (b) Zoomed-in SEM image of the topological interface. The red line represents the topological interface, the blue hexagon indicates a unit cell in the topological photonic crystal, and the orange hexagon indicates a unit cell in the trivial photonic crystal. (c) Calculated discrete cavity modes of the topological vortex laser (red and green dots). Gray curves are the calculated bulk bands of the topological photonic crystal. Black lines indicate the Dirac cone of an infinite long topological interface. (d) Schematic of the dispersion curves of the topological edge modes and conventional whispering gallery modes. Topological edge state lasing requires no in-plane momentum in principle, which decouples the radiation direction from the resonant plane. In contrast, the dominant radiation field of the conventional whispering gallery modes is in plane and omnidirectional due to momentum conservation. (e) Schematic of the topological vortex laser with circularly polarized vortex beam far-field radiation. The near-field spin and orbital angular momentum have a one-to-one far-field radiation correspondence.

which provides a more flexible and robust way to construct a nanophotonics platform. We construct the two photonic crystals aside of topological interface distinct in topology but with a common bulk bandgap via deformed honeycomb lattices [42]. It is well known that such a topological interface supports two spin-momentum-locked edge states of opposite momenta with opposite spins [72–75]. The two edge states lying in the bulk band gap are with dispersion of a Dirac cone centered at the Γ point in the Brillouin zone [42].

In the topological vortex laser cavity, the edge states become discrete due to the finite cavity side length [Fig. 1(c)]. These discrete edge states propagate along the topological interface and are immune to bending and defects, which forms an effective cavity resonance indicated by the red line and arrows in Fig. 1(a). Such a topologically protected cavity resonance requires no large in-plane momentum, which decouples the radiation direction from the resonant plane resulting in directional surface emitting. As shown in Fig. 1(d), the edge modes locate in the center of the light cone with near zero in-plane wave vector. This is in stark contrast to conventional cavities where the dominant wave vector is in the resonant plane to acquire effective feedback. Figure 1(d) also shows the dispersion curve of a conventional whispering gallery mode resonator. Because of the requirement of total internal reflection, the in-plane wave vectors of the resonant modes are larger than free space wave vectors, thereby, the dominant radiation field of these modes is in plane and omnidirectional due to momentum conservation.

A spin-momentum-locked edge state is a propagating wave free from coupling to its counterpropagating counterpart, which results in a uniform intensity distribution along the resonance loop. When pumped for lasing, such a mode will experience no spatial hole burning and can saturate gain to prevent other modes from lasing, which lifts degeneracy of the paired counterpropagating spin-momentum-locked edge modes. The properties of a lasing single spin-momentum-locked edge mode can be probed via its far field radiation. Because of the conservation of angular momentum, the circular polarization and vortex of the far field radiation represent the near-field spin and orbital angular momentum of the edge mode respectively [Fig. 1(e)].

Lasing evidences of the topological vortex laser.—Figure 2(a) shows the spontaneous and lasing emission spectra of a topological vortex laser under optical pumping

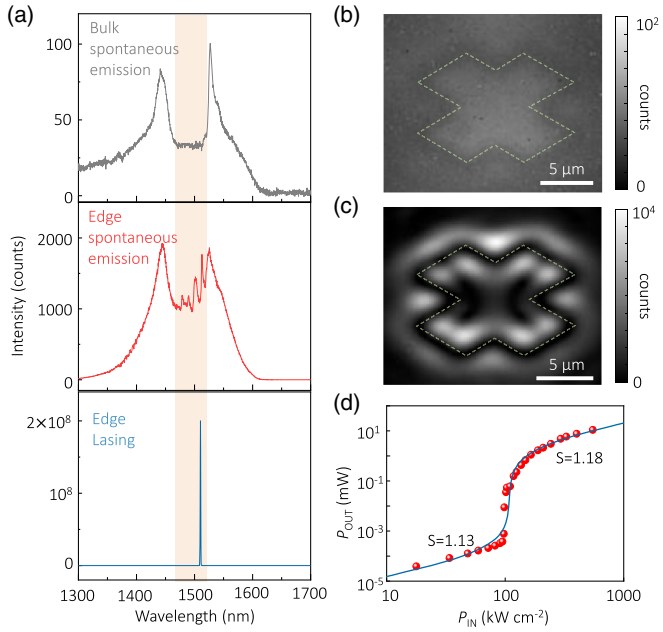

FIG. 2. Lasing evidences of the topological vortex laser. (a) Upper: Spontaneous emission spectrum obtained from a bulk photonic crystal region. The spectrum shows a clear suppressed intensity gap induced by a photonic band gap indicated by the orange region. Middle: Spontaneous emission spectrum of the topological interface, showing pronounced resonant peaks within the band gap. Bottom: lasing spectrum of the vortex laser under a pump power of 545 kW cm^{-2}. (b) Spontaneous emission pattern. (c) Lasing emission pattern. In (b) and (c), dashed green line indicates the ⋈-shaped topological interface. (d) Integrated output power as a function of pump intensity in log scale. The slope in the spontaneous emission state and lasing state is 1.13 and 1.18, respectively. Dots, data; curve, fitting.

at room temperature [42]. At a spontaneous emission state, four pronounced resonant peaks appear inside the photonic bandgap. At each cavity resonance wavelength, the edge state modes are twofold degenerate with two spin-momentum locked modes of $|l,+\rangle$ and $|-l,-\rangle$, where l denotes orbital angular momentum, $+$ and $-$ denote spin-up and spin-down, respectively [42]. In contrast, when only a bulk photonic crystal region is pumped, the spectrum shows a band gap modulated MQWs spontaneous emission with a bandwidth of about 50 nm, and there is no resonant peak inside the photonic band gap [42]. Above the lasing threshold, single mode lasing occurs at the wavelength of 1510.5 nm. The linewidth of the lasing mode is only about 0.4 nm, much narrower than the same mode at spontaneous emission state (~3.1 nm) [42].

The lasing effect is also evidenced by the transition of the emission patterns below and above the lasing threshold. As shown in Figs. 2(b) and 2(c), although pumped by the same laser beam, the lasing emission pattern is well defined and predominantly locates near the topological interface, while the spontaneous emission pattern is nearly uniform as the superposition of all available optical modes. Interestingly, in the lasing pattern, the emission at the topological interface is strongly suppressed appearing as a dark "⋈", which is due to a destructive interference between the emissions from the topological region and the trivial region aside [42]. We also measure the light-light curve of the device, which shows a clearly "S"-shaped in log scale indicating a phase transition from spontaneous emission to lasing emission as shown in Fig. 2(d). The threshold power density of the device is ~120 kW cm^{-2} [42].

Out-of-plane radiation feature of the lasing spin-momentum-locked edge mode.—Topological edge state lasing requires no in-plane momentum in principle, which decouples the radiation direction from the resonant plane. The directionally surface emitting feature of the topological vortex laser is shown in the momentum space image of the lasing beam [Fig. 3(a)], which is a donut-shaped pattern centered at zero in-plane wave vector point (Γ point in the Brillouin zone). The donut is with a radius of ~3.39° [42]. Figure 3(b) shows the full wave simulated pattern of the $|-2,+\rangle$ mode, which matches well with the experimental one [42].

The near-field spin and orbital angular momentum of the topological vortex laser have a one-to-one far-field radiation correspondence as shown in the schematic of Fig. 3(c). For a spin-momentum-locked edge mode, all the unit cells share the same spin direction. Because of the subwavelength scale of the unit cell, the spin in each unit cell acts as an emission source with circular polarization [76], the superposition of which leads to a circularly polarized far field radiation. For the mode with $l=0$, the phase shift between neighboring cells is zero and all the cells oscillate with the same spin, leading to a pure circularly polarized radiation without orbital angular momentum. Otherwise, due to the traveling phase, spins between neighboring cells have a certain phase shift, which gives a spiral-shaped gradient phase front of the emission beam along the closed resonance loop. In the far field, such a gradient phase front forms the vortex radiation of the spin-momentum-locked edge mode. We note that the lasing emission could also be used to probe other exotic phenomena with topology origin [77].

Figure 3(d) shows the lasing emission intensity after a linear polarizer with varied polarization angles, which indicates that the intensity is insensitive to the polarization angle. Adding a quarter-wave plate before the linear polarizer, the polarization dependent intensity distribution indicates that the emission beam becomes linearly polarized. Based on these experiments, we confirm that the laser emission is a left-handed circularly polarized $|-2,+\rangle$ mode [42].

We then measure the orbital angular momentum of the lasing beam by self-interference utilizing a shearing interferometer. The interference pattern exhibits two fork-shaped patterns as shown in Fig. 3(e), where the two red stars at the dislocation indicate the phase singularities of the

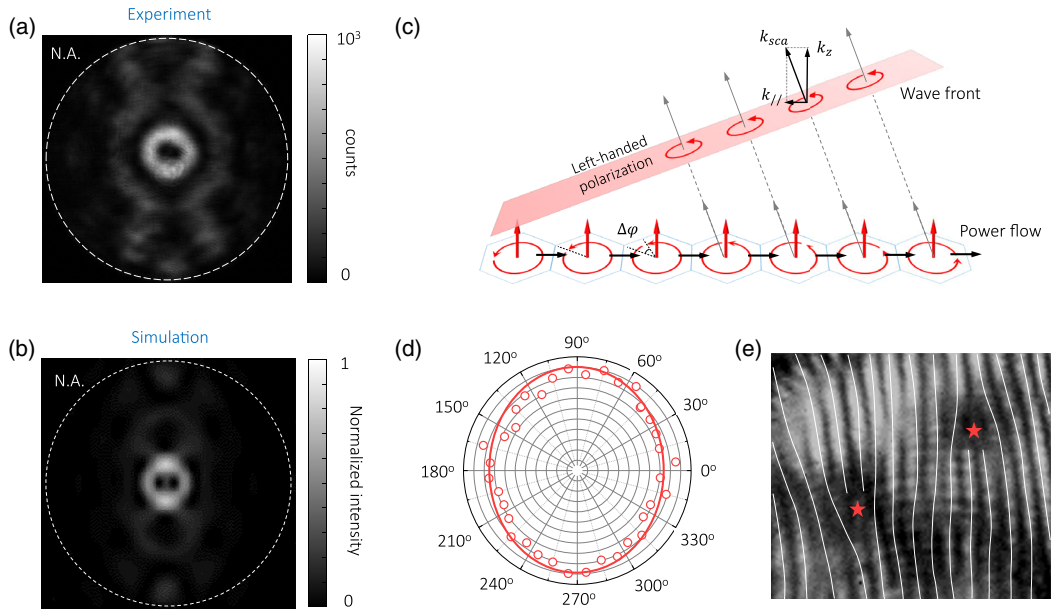

FIG. 3. Out-of-plane radiation feature of the lasing spin-momentum-locked edge mode. (a)–(b) Momentum space patterns of the lasing beam obtained from experiment (a) and full wave simulation (b). The white dashed circles in (a) and (b) indicate the numerical aperture of the collection objective. (c) Schematic of the laser emission from a spin-momentum-locked topological edge mode. The near-field spin and orbital angular momentum has a one-to-one far-field radiation correspondence. (d) Lasing emission intensity after a linear polarizer with varied polarization angles. Adding a quarter-wave plate before the linear polarizer, the emission beam will become linearly polarized. (e) Off-center self-interference of the lasing beam, showing two fork-shaped patterns located near two phase singularities (marked with red stars), which indicates that the laser emission is a vortex beam with a topological charge of −2, corresponding to the azimuthal order of the cavity mode.

two split laser emission beams, respectively. At each singularity, the intensity of the interference pattern decreases to zero, and there is a transition of two fringes becoming four, which indicates that the laser emission is a vortex beam with a topological charge of −2, corresponding to the azimuthal order of the cavity mode [42]. We have also observed a topological vortex laser emitting vortex radiation with a topological charge of 1, the results of which are shown in the Supplemental Material Part 15 [42].

Direct evidence of backscattering free and high side-mode suppression ratio.—In our topological cavity, the immunity of coupling between the two degenerate spin-momentum locked edge states is protected by C_{6v} symmetry. Experimentally, we verify this distinct feature of topological edge states by measuring the lasing emission wavelengths of the two spin-momentum locked edge states of opposite momenta with opposite spins. The coupling strength of the two modes is proportional to the split of their lasing wavelengths.

Figure 4(a) shows the lasing spectra of the two edge states of opposite momenta with opposite spins. They have exactly the same emission wavelength, which indicates that there is no coupling between the two edge states despite the strongly irregular cavity shape. Figure 4(b) shows the self-interference pattern of the $|2,-\rangle$ mode measured by the shearing interferometer in the momentum space. The pattern is similar to the one of $|-2,+\rangle$ shown in Fig. 3(e) but with

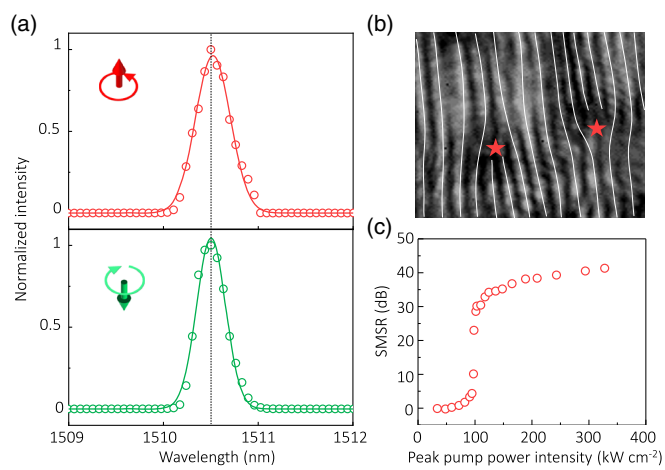

FIG. 4. Direct evidence of backscattering free and high side-mode suppression ratio. (a) Lasing spectra of the two edge states of opposite momenta with opposite spins. The identical emission wavelength indicates that there is no coupling between the two modes despite the strongly irregular cavity shape. (b) Self-interference pattern of the $|2,-\rangle$ mode [bottom panel in (a)] measured by the shearing interferometer in the momentum space. The pattern is similar to the one of $|-2,+\rangle$ shown in Fig. 3(e) but with flipped fork-shaped patterns which indicate that the signs of orbital angular momenta of the two modes are opposite. (c) Side-mode suppression ratio (SMSR) versus the pump intensity, where we can see that the side-mode suppression ratio increases dramatically with the onset of lasing.

flipped fork-shaped pattern which indicates that the signs of orbital angular momentums of the two modes are opposite [42]. Although the patterns of the $|-2,+\rangle$ and $|2,-\rangle$ modes are same, we find that they can be selectively excited by slight modification of pump beam position, which is due to the spontaneous emission fluctuation induced symmetry broken in the onset of the lasing process.

The uniform intensity distribution along the resonance loop of the traveling mode lasing experiences no spatial hole burning effect and saturates gain to prevent other modes from lasing. Consequently, our topological vortex laser has a side-mode suppression ratio as high as 42 dB [42], a record value among reported micro- and nanoscale lasers [42]. Figure 4(c) shows the side-mode suppression ratio versus the pump intensity, where we can see that the side-mode suppression ratio increases dramatically with the onset of lasing.

Conclusion.—We reveal a nontrivial out-of-plane radiation feature of a topological insulator edge state. In a non-Hermitian topological photonic system, we demonstrate a topological vortex laser operating on a single spin-momentum-locked edge mode. The topological edge state lasing requires no in-plane momentum in principle, which decouples the radiation direction from the resonant plane. The directionally surface emitting feature is shown as a donut-shaped pattern with a radius of ~3.39° centered at zero in-plane wave vector point in the momentum space. Our results indicate that the lasing process has a striking effect to the topological insulator by lifting the degeneracy of the paired counterpropagating spin-momentum-locked edge modes. The topological edge state lasing experiences no spatial hole burning and saturates gain to prevent other modes from lasing, resulting in a side-mode suppression ratio as high as 42 dB. The resonance mechanism can apply to other non-Hermitian wave systems, and the methodology of probing a near-field topology feature by far-field lasing emission can be used to study other exotic phenomena. The topological vortex laser device can lead to applications in superresolution imaging, optical tweezers, free-space optical sensing, and communication.

This work is supported by the National Natural Science Foundation of China (Grants No. 91950115, No. 11774014, and No. 61521004), Beijing Natural Science Foundation (Grant No. Z180011) and the National Key R&D Program of China (Grant No. 2018YFA0704401).

*To whom all correspondence should be addressed.
renminma@pku.edu.cn

[1] J. E. Moore, The birth of topological insulators, Nature (London) **464**, 194 (2010).
[2] H. Beidenkopf, P. Roushan, J. Seo, L. Gorman, I. Drozdov, Y. S. Hor, R. J. Cava, and A. Yazdani, Spatial fluctuations of helical Dirac fermions on the surface of topological insulators, Nat. Phys. **7**, 939 (2011).
[3] Y. Xu, D. D. Awschalom, and J. Nitta, *Handbook of Spintronics* (Springer, Dordrecht, The Netherlands, 2016).
[4] X. L. Qi and S. C. Zhang, Topological insulators and superconductors, Rev. Mod. Phys. **83**, 1057 (2011).
[5] M. Z. Hasan and C. L. Kane, Colloquium: Topological insulators, Rev. Mod. Phys. **82**, 3045 (2010).
[6] X. L. Qi, T. L. Hughes, and S. C. Zhang, Topological field theory of time-reversal invariant insulators, Phys. Rev. B **78**, 195424 (2008).
[7] A. P. Schnyder, S. Ryu, A. Furusaki, and A. W. W. Ludwig, Classification of topological insulators and superconductors in three spatial dimensions, Phys. Rev. B **78**, 195125 (2008).
[8] A. M. Essin, J. E. Moore, and D. Vanderbilt, Magnetoelectric Polarizability and Axion Electrodynamics in Crystalline Insulators, Phys. Rev. Lett. **102**, 146805 (2009).
[9] L. Fu and C. L. Kane, Probing Neutral Majorana Fermion Edge Modes with Charge Transport, Phys. Rev. Lett. **102**, 216403 (2009).
[10] A. R. Akhmerov, J. C. Nilsson, and C. W. J. Beenakker, Electrically Detected Interferometry of Majorana Fermions in a Topological Insulator, Phys. Rev. Lett. **102**, 216404 (2009).
[11] D. Hsieh, Y. Xia, D. Qian, L. Wray, J. H. Dil, F. Meier, J. Osterwalder, L. Patthey, J. G. Checkelsky, N. P. Ong *et al.*, A tunable topological insulator in the spin helical Dirac transport regime, Nature (London) **460**, 1101 (2009).
[12] J. Han, A. Richardella, S. A. Siddiqui, J. Finley, N. Samarth, and L. Liu, Room-temperature spin-orbit torque switching induced by a topological insulator, Phys. Rev. Lett. **119**, 077702 (2017).
[13] S. Raghu and F. D. M. Haldane, Analogs of quantum-Hall-effect edge states in photonic crystals, Phys. Rev. A **78**, 033834 (2008).
[14] F. D. M. Haldane and S. Raghu, Possible realization of directional optical waveguides in photonic crystals with broken time-reversal symmetry, Phys. Rev. Lett. **100**, 013904 (2008).
[15] L. Lu, J. D. Joannopoulos, and M. Soljačić, Topological photonics, Nat. Photonics **8**, 821 (2014).
[16] A. B. Khanikaev and G. Shvets, Two-dimensional topological photonics, Nat. Photonics **11**, 763 (2017).
[17] T. Ozawa, H. M. Price, A. Amo, N. Goldman, M. Hafezi, L. Lu, M. C. Rechtsman, D. Schuster, J. Simon, O. Zilberberg *et al.*, Topological photonics, Rev. Mod. Phys. **91**, 015006 (2019).
[18] P. Lodahl, S. Mahmoodian, S. Stobbe, A. Rauschenbeutel, P. Schneeweiss, J. Volz, H. Pichler, and P. Zoller, Chiral quantum optics, Nature (London) **541**, 473 (2017).
[19] K. Y. Bliokh, F. J. Rodríguez-Fortuño, F. Nori, and A. V. Zayats, Spin-orbit interactions of light, Nat. Photonics **9**, 796 (2015).
[20] S. Barik, A. Karasahin, C. Flower, T. Cai, H. Miyake, W. DeGottardi, M. Hafezi, and E. Waks, A topological quantum optics interface, Science **359**, 666 (2018).
[21] J. S. Pan, X. J. Liu, W. Zhang, W. Yi, and G. C. Guo, Topological superradiant states in a degenerate Fermi gas, Phys. Rev. Lett. **115**, 045303 (2015).
[22] M. Bello, G. Platero, J. I. Cirac, and A. González-Tudela, Unconventional quantum optics in topological waveguide QED, Sci. Adv. **5**, eaaw0297 (2019).

[23] H. Pichler, T. Ramos, A. J. Daley, and P. Zoller, Quantum optics of chiral spin networks, Phys. Rev. A **91**, 042116 (2015).

[24] A. Metelmann and A. A. Clerk, Nonreciprocal Photon Transmission and Amplification via Reservoir Engineering, Phys. Rev. X **5**, 021025 (2015).

[25] A. Blanco-Redondo, B. Bell, D. Oren, B. J. Eggleton, and M. Segev, Topological protection of biphoton states, Science **362**, 568 (2018).

[26] M. Hafezi, E. A. Demler, M. D. Lukin, and J. M. Taylor, Robust optical delay lines with topological protection, Nat. Phys. **7**, 907 (2011).

[27] M. Hafezi, S. Mittal, J. Fan, A. Migdall, and J. M. Taylor, Imaging topological edge states in silicon photonics, Nat. Photonics **7**, 1001 (2013).

[28] Y. Yang, Y. F. Xu, T. Xu, H. X. Wang, J. H. Jiang, X. Hu, and Z.-H. Hang, Visualization of a Unidirectional Electromagnetic Waveguide using Topological Photonic Crystals made of Dielectric Materials, Phys. Rev. Lett. **120**, 217401 (2018).

[29] A. I. Shalaev, W. Walasik, A. Tsukernik, Y. Xu, and N. M. Litchinitser, Robust topologically protected transport in photonic crystals at telecommunication wavelengths, Nat. Nanotechnol. **14**, 31 (2019).

[30] G. Siroki, P. A. Huidobro, and V. Giannini, Topological photonics: From crystals to particles, Phys. Rev. B **96**, 041408(R) (2017).

[31] C. Y. Ji, G. B. Liu, Y. Zhang, B. Zou, and Y. Yao, Transport tuning of photonic topological edge states by optical cavities, Phys. Rev. A **99**, 043801 (2019).

[32] Y. T. Yang and Z. H. Hang, Topological whispering gallery modes in two-dimensional photonic crystal cavities, Opt. Express **26**, 21235 (2018).

[33] M. A. Bandres, S. Wittek, G. Harari, M. Parto, J. Ren, M. Segev, D. N. Christodoulides, and M. Khajavikhan, Topological insulator laser: Experiments, Science **359**, eaar4005 (2018).

[34] G. Harari, M. A. Bandres, Y. Lumer, M. C. Rechtsman, Y. D. Chong, M. Khajavikhan, D. N. Christodoulides, and M. S. Harari, Topological insulator laser: Theory, Science **359**, eaar4003 (2018).

[35] H. Zhao, X. Qiao, T. Wu, B. Midya, S. Longhi, and L. Feng, Non-Hermitian topological light steering, Science **365**, 1163 (2019).

[36] D. Leykam, K. Y. Bliokh, C. L. Huang, Y. D. Chong, and F. Nori, Edge Modes, Degeneracies, and Topological Numbers in Non-Hermitian Systems, Phys. Rev. Lett. **118**, 040401 (2017).

[37] H. Shen, B. Zhen, and L. Fu, Topological Band Theory for Non-Hermitian Hamiltonians, Phys. Rev. Lett. **120**, 146402 (2018).

[38] K. Takata and M. Notomi, Photonic Topological Insulating Phase Induced Solely by Gain And Loss, Phys. Rev. Lett. **121**, 213902 (2018).

[39] F. Song, S. Y. Yao, and Z. Wang, Non-Hermitian Topological Invariants in Real Space, Phys. Rev. Lett. **123**, 246801 (2019).

[40] S. Yao and Z. Wang, Edge States and Topological Invariants of Non-Hermitian Systems, Phys. Rev. Lett. **121**, 086803 (2018).

[41] K. Kawabata, K. Shiozaki, M. Ueda, and M. Sato, Symmetry and Topology in Non-Hermitian Physics, Phys. Rev. X **9**, 041015 (2019).

[42] See Supplemental Material at http://link.aps.org/supplemental/10.1103/PhysRevLett.125.013903 for the detailed discussions and experimental results: comparison table of topological vortex laser with representative small lasers, which includes Refs. [33,43–72]; device fabrication; design and numerical simulation of photonic crystals and devices; band structure of edge states; optical characterization; cavity modes in topological vortex laser; spontaneous emission spectra of photonic crystals; linewidth of the lasing edge mode in spontaneous emission spectrum; lasing emission suppression at topological interfaces; threshold of topological vortex laser; directionality of lasing beam; polarization and orbital angular momentum characterization; self-interference patterns of vortex beam carrying opposite orbital angular momentum; characterization of the $\ell = 1$ mode; side-mode suppression ratio.

[43] B. Bahari, A. Ndao, F. Vallini, A. El Amili, Y. Fainman, and B. Kanté, Nonreciprocal lasing in topological cavities of arbitrary geometries,, Science **358**, 636 (2017).

[44] H. Zhao, P. Miao, M. H. Teimourpour, S. Malzard, R. El-Ganainy, H. Schomerus, and L. Feng, Topological hybrid silicon microlasers, Nat. Commun. **9**, 981 (2018).

[45] P. St-Jean, V. Goblot, E. Galopin, A. Lemaître, T. Ozawa, L. Le Gratiet, I. Sagnes, J. Bloch, and A. A. St-Jean, Lasing in topological edge states of a one-dimensional lattice, Nat. Photonics **11**, 651 (2017).

[46] M. Parto, S. Wittek, H. Hodaei, G. Harari, M. A. Bandres, J. Ren, M. C. Rechtsman, M. Segev, D. N. Christodoulides, and M. Khajavikhan, Edge-Mode Lasing in 1D Topological Active Arrays, Phys. Rev. Lett. **120**, 113901 (2018).

[47] Commercial 4 Gbps 1550 nm single mode VCSEL, RayCan Co., Ltd. in Korea, http://www.raycan.com/.

[48] Commercial 10 Gbps 850 nm multimode VCSEL, Global Communication Semiconductors, LLC. in California, http://www.gcsincorp.com/.

[49] I. Hameeda, M. A. H. Ahmed, and K. Fumio, Single-mode double transverse cavity VCSEL, in *24th Microoptics Conference* (2019).

[50] X. Gu, M. Nakahama, A. Matsutani, M. Ahmed, A. Bakry, and F. Koyama, 850 nm transverse-coupled-cavity vertical-cavity surface-emitting laser with direct modulation bandwidth of over 30 GHz, Appl. Phys. Express **8**, 082702 (2015).

[51] A. Kodigala, T. Lepetit, Q. Gu, B. Bahari, Y. Fainman, and B. Kanté, Lasing action from photonic bound states in continuum, Nature (London) **541**, 196 (2017).

[52] S. T. Ha, Y. H. Fu, N. K. Emani, Z. Pan, R. M. Bakker, R. P. Domínguez, and A. I. Kuznetsov, Directional lasing in resonant semiconductor nanoantenna arrays, Nat. Nanotechnol. **13**, 1042 (2018).

[53] H. Altug and J. Vučković, Photonic crystal nanocavity array laser, Opt. Express **13**, 8819 (2005).

[54] T. Watanabea, H. Abe, Y. Nishijima, and T. Baba, Array integration of thousands of photonic crystal nanolasers, Appl. Phys. Lett. **104**, 121108 (2014).

[55] D. Wang, A. Yang, W. Wang, Y. Hua, R. D. Schaller, G. C. Schatz, and T. W. Odom, Band-edge engineering

for controlled multi-modal nanolasing in plasmonic superlattices, Nat. Nanotechnol. **12**, 889 (2017).

[56] A. Yang, Z. Li, M. P. Knudson, A. J. Hryn, W. Wang, K. Aydin, and T. W. Odom, Unidirectional lasing from template-stripped two-dimensional plasmonic crystals, ACS Nano **9**, 11582 (2015).

[57] D. Wang, M. R. Bourgeois, W. Lee, R. Li, D. Trivedi, M. P. Knudson, W. Wang, G. C. Schatz, and T. W. Odom, Stretchable nanolasing from hybrid quadrupole plasmons, Nano Lett. **18**, 4549 (2018).

[58] F. van Beijnum, P. J. van Veldhoven, E. J. Geluk, M. J. A. de Dood, G. W. Hooft, and M. P. van Exter, Surface Plasmon Lasing Observed in Metal Hole Arrays, Phys. Rev. Lett. **110**, 206802 (2013).

[59] P. Mechet, T. Spuesens, S. Werquin, K. Vandoorne, N. Olivier, N. Olivier, P. Regreny, D. Van Thourhout, D. Van Thourhout, and G. Morthier, All-optical low-power 2R regeneration of 10-Gb/s NRZ signals using a III-V on SOI microdisk laser, IEEE Photonics J. **5**, 7802510 (2013).

[60] X. W. Ma, Y. Z. Huang, L. X. Zou, B. W. Liu, H. Long, H. Z. Weng, Y. D. Yang, and J. L. Xiao, Narrow-linewidth microwave generation using AlGaInAs/InP microdisk lasers subject to optical injection and optoelectronic feedback, Opt. Express **23**, 20321 (2015).

[61] V. Kryzhanovskaya, E. I. Moiseev, F. I. Zubov, A. M. Mozharov, M. V. Maximov, N. A. Kalyuzhnyy, S. A. Mintairov, M. M. Kulagina, S. A. Blokhin, K. E. Kudryavtsev *et al.*, Direct modulation characteristics of microdisk lasers with InGaAs/GaAs quantum well-dots, Photonics Res. **7**, 664 (2019).

[62] E. Moiseev, N. Kryzhanovskaya, M. Maximov, F. Zubov, A. Nadtochiy, M. Kulagina, Y. Zadiranov, N. Kalyuzhnyy, S. Mintairov, and A. Zhukov, Highly efficient injection microdisk lasers based on quantum well-dots, Opt. Lett. **43**, 4554 (2018).

[63] Y. Yu, W. Xue, E. Semenova, K. Yvind, and J. Mork, Demonstration of a self-pulsing photonic crystal Fano laser, Nat. Photonics **11**, 81 (2017).

[64] H. Jang, I. Karnadi, P. Pramudita, J. H. Song, K. S. Kim, and Y. H. Lee, Sub-microWatt threshold nanoisland lasers, Nat. Commun. **6**, 8276 (2015).

[65] J. Lee, I. Karnadi, J. T. Kim, Y. Lee, and M. Kim, Printed nanolaser on silicon, ACS Photonics **4**, 2117 (2017).

[66] P. Hamel, S. Haddadi, F. Raineri, P. Monnier, G. Beaudoin, I. Sagnes, A. Levenson, and A. M. Yacomotti, Spontaneous mirror-symmetry breaking in coupled photonic-crystal nanolasers, Nat. Photonics **9**, 311 (2015).

[67] M. Yoshida, M. De Zoysa, K. Ishizaki, Y. Tanaka, M. Kawasaki, R. Hatsuda, B. Song, J. Gelleta, and S. Noda, Double-lattice photonic-crystal resonators enabling high-brightness semiconductor lasers with symmetric narrow-divergence beams, Nat. Mater. **18**, 121 (2019).

[68] S. Wang, H. Z. Chen, and R. M. Ma, High performance plasmonic nanolasers with external quantum efficiency exceeding 10%, Nano Lett. **18**, 7942 (2018).

[69] E. I. Galanzha, R. Weingold, D. A. Nedosekin, M. Sarimollaoglu, J. Nolan, W. Harrington, A. S. Kuchyanov, R. G. Parkhomenko, F. Watanabe *et al.*, Spaser as a biological probe, Nat. Commun. **8**, 15528 (2017).

[70] K. Ding, M. T. Hill, Z. C. Liu, L. J. Yin, P. J. van Veldhoven, and C. Z. Ning, Record performance of electrical injection sub-wavelength metallic-cavity semiconductor lasers at room temperature, Opt. Express **21**, 4728 (2013).

[71] Y. Kyoungsik, A. Lakhani, and M. Wu, Subwavelength metal-optic semiconductor nanopatch lasers, Opt. Express **18**, 8790 (2010).

[72] Z. K. Shao, H. Z. Chen, S. Wang, X. R. Mao, Z. Q. Yang, S. L. Wang, X. X. Wang, X. Hu, and R. M. Ma, A high-performance topological bulk laser based on band-inversion-induced reflection, Nat. Nanotechnol. **15**, 67 (2020).

[73] L. H. Wu and X. Hu, Scheme for Achieving a Topological Photonic Crystal by Using Dielectric Material, Phys. Rev. Lett. **114**, 223901 (2015).

[74] S. Barik, H. Miyake, W. DeGottardi, E. Waks, and M. Hafezi, Two-dimensionally confined topological edge states in photonic crystals, New J. Phys. **18**, 113013 (2016).

[75] L. Wu and X. Hu, Topological properties of electrons in honeycomb lattice with detuned hopping energy, Sci. Rep. **6**, 24347 (2016).

[76] J. B. Zhu, Y. J. Chen, Y. F. Zhang, X. L. Cai, and S. Y. Yu, Spin and orbital angular momentum and their conversion in cylindrical vector vortices, Opt. Lett. **39**, 4435 (2014).

[77] C. Guo, M. Xiao, Y. Guo, L. Yuan, and S. Fan, Meron Spin Textures in Momentum Space, Phys. Rev. Lett. **124**, 106103 (2020).